RESEARCH ARTICLE

Macromolecular Rapid Communications
www.mrc-journal.de

Hydrolyzable Poly(β-thioether ester ketal) Thermosets via Acyclic Ketal Monomers

*Benjamin M. Alameda, Joseph Scott Murphy, Bernardo L. Barea-López, Karly D. Knox, Jonathan D. Sisemore, and Derek L. Patton**

Hydrolytically degradable poly(β-thioether ester ketal) thermosets are synthesized via radical-mediated thiol-ene photopolymerization using three novel dialkene acyclic ketal monomers and a mercaptopropionate based tetrafunctional thiol. For all thermoset compositions investigated, degradation behavior is highly tunable based on the structure of the incorporated ketal and pH. Complete degradation of the thermosets is observed upon exposure to acidic and neutral pH, and under high humidity conditions. Polymer networks composed of cross-link junctions based on acyclic dimethyl ketals degrade the quickest, whereas networks containing acyclic cyclohexyl ketals undergo hydrolytic degradation on a longer timescale. Thermomechanical analysis reveals low glass transition temperatures and moduli typical of thioether-based thermosets.

1. Introduction

Polymer thermosets with hydrolyzable motifs in the backbone of the polymer network have enabled many technologies (e.g., lithography, drug delivery, and regenerative medicine)[1] and offer potential to advance the utility of environment-friendly materials for numerous applications such as adhesives and composites. Deconstruction of the thermoset is achieved via hydrolysis of labile functional groups (e.g., esters,[2–4] acetals,[2–4] ketals,[5–8] and anhydrides[9,10]) within the polymer network—a process that yields macromolecular and/or small molecule by-products where the distribution of products is dependent on both monomer design and the mechanism (chain-growth or step-growth) by which the network is constructed.[11]

Ketals are particularly interesting for the design of degradable thermosets due to their relative ease of synthesis, the variety of ketone building blocks from which ketals can be prepared, and their sensitivity toward hydrolysis in acidic/neutral pH conditions. In contrast to thermosets derived from esters and anhydrides, which degrade into acidic by-products, hydrolysis of ketal-based thermosets yields neutral ketone and alcohol by-products.[12] Ketal-based thermosets are further discerned from their ester and anhydride-derived counterparts due to their excellent stability under basic pH conditions. Ketals undergo hydrolysis via a well-established mechanism in which the formation of the resonance-stabilized carbenium ion intermediate serves as the rate-determining step.[12] Consequently, the hydrolytic stability of ketals is highly tunable based on steric and electronic effects that are well established in the literature.[4,7,8,13,14] For example, Kreevoy et al. established fundamental hydrolysis rates of acyclic ketals based on differences in steric or torsional strains induced by the parent ketal ring size or α-substituent size, where a higher degree of inherent strain resulted in faster rates of hydrolysis.[15] While these principles have been extensively applied to the investigation of linear[16–21] and branched[19,22–40] polyketals, the exploration of ketal-based thermosets has received much less attention with much of the recent focus falling on hydrogels.[31,41–45] Furthermore, the structural diversity of ketal-based cross-linkers has been limited mostly to acyclic dimethyl ketals.[15,19,25] Liu et al. published an extensive library of acyclic ketal-based cross-linkers demonstrating the ability to use substituent effects to broadly tune the encapsulation stability of polymer nanogels.[19] More recently, we showed the influence of monomer structure on the degradation of hydrophilic poly(β-thioether ester ketal) networks composed of cyclic diketals. While these materials provided access to photopolymer thermosets with tunable degradation profiles, the diversity and availability of cyclic diketone precursors are limited.

Herein, we report the synthesis of degradable poly(β-thioether ester ketal) networks via thiol-ene photopolymerization using three novel bis-allyl acyclic ketal monomers derived from acetone, cyclopentanone, and cyclohexanone. The monomers were designed using the aforementioned commercially available ketones and allyl alcohol to form dimethyl, cyclopentyl, and cyclohexyl ketal diallyl cross-linkers. The step-growth mechanism of thiol-ene photopolymerization enables the synthesis of homogenous polymer networks with the insertion of a hydrolytically labile ketal at each cross-link junction, allowing for complete and controlled network degradation into charge-neutral ketone and alcohol by-products in a variety of pH solutions. Degradation of each network was quantified via mass-loss degradation experiments with overall network stability dictated by ketal structure

B. M. Alameda, J. S. Murphy, B. L. Barea-López, K. D. Knox, J. D. Sisemore, D. L. Patton
School of Polymer Science and Engineering
University of Southern Mississippi
118 College Drive #5050, Hattiesburg, MS 39406, USA
E-mail: derek.patton@usm.edu

The ORCID identification number(s) for the author(s) of this article can be found under https://doi.org/10.1002/marc.202200028

DOI: 10.1002/marc.202200028

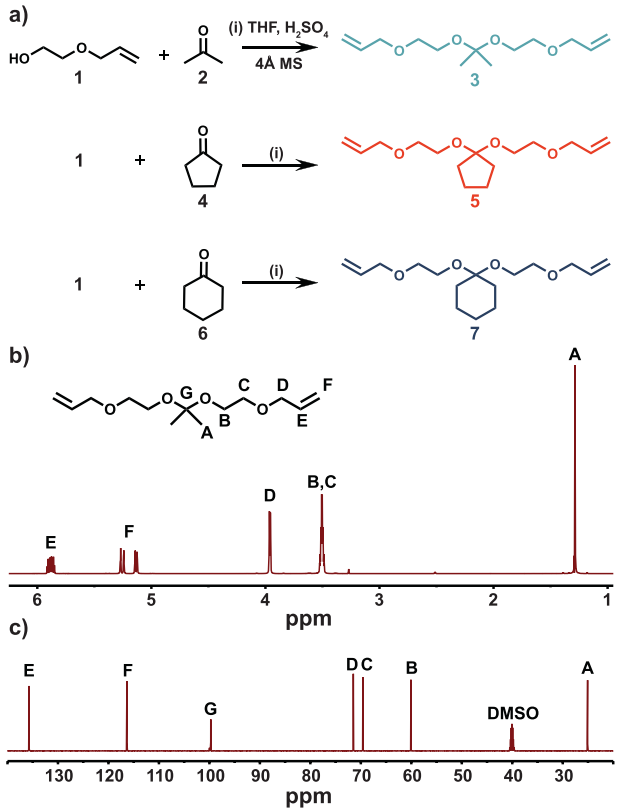

Figure 1. a) Synthesis scheme of acyclic ketal monomers 3, 5, and 7 from the acid-catalyzed ketalization of acetone (2), cyclopentanone (4), cyclohexanone (6), and 2-allyloxyethanol (1).1H NMR b) and13C NMR c) of monomer 3 with chemical signal assignments.

and solution pH. Additionally, the mechanical and thermomechanical properties of each network were measured to elucidate trends based on monomer structure.

2. Results and Discussion

2.1. Monomer Synthesis

Our initial goal was to construct a library of accessible alkene-functionalized ketal monomers to be used as building blocks for degradable thiol-ene networks. Acetone, cyclopentanone, and cyclohexanone were chosen as starting reagents for the synthesis of monomers 3, 5, and 7, respectively. The synthesis procedure was similar for each monomer and consisted of a simple one-step, acid-catalyzed ketalization of 2-allyloxyethanol and the chosen ketones using an H_2SO_4 catalyst and 4 Å molecular sieves to uptake water produced by the reaction (**Figure 1**a). Yields of 15.9%, 10.9%, and 22.7% were obtained for monomers 3, 5, and 7, respectively, with the highest yield attributed to the cyclohexyl-based ketal due to its enhanced stability.

The structure and purity of all monomers were analyzed by ^{1}H NMR,^{13}C NMR, COSY, HSQC, and HRMS NMR experiments (Figures S1–12, Supporting Information). Figure 1b shows an example of ^{1}H NMR spectra for monomer 3 with expected signals of the unsaturated allyl protons (E, F), allylic protons (D), CH_2 protons (B,C), and dimethyl protons (A). The ^{13}C-NMR of monomer 3 is shown in Figure 1c and exhibits a distinctive quaternary carbon signal (G) at 99.73 ppm with unsaturated allyl carbons at 116.35 ppm (F) and 135.72 ppm (E). Elucidation of specific proton signals and splitting was made possible by supplementary COSY (^{1}H–^{1}H) and HSQC (^{1}H–^{13}C) 2D NMR experiments. Identical NMR experiments were employed to elucidate the structures of monomers 5 and 7. Additionally, mass spectrometry was employed to identify the mass to charge ratio (m/z) for all investigated monomers and confirm each structure's molecular weight.

2.2. Monomer Hydrolysis Kinetics

To explore the stability of the ketal-based linkages, we initially probed the hydrolysis kinetics of the three monomers under acidic and neutral conditions. Stability under basic conditions was also initially assessed; however, hydrolysis of ketals under basic conditions is known to be extremely suppressed.[12] As shown in Figures S13–15 (Supporting Information), we observed no evidence of ketal hydrolysis for monomers 3, 5, and 7 even at extended times (e.g., 194 days); thus, detailed kinetic profiles were not collected under basic conditions. Hydrolysis kinetics for each monomer was measured via^{1}H-NMR experiments using CD_3CN/D_2O buffers of pD 5.0 (pH 4.6) and pD 7.4 (pH 7.0). A 0.01875 M monomer solution in CD_3CN/D_2O buffer (75:25 v/v) was utilized to fully solubilize the starting ketal monomers and the by-products upon hydrolysis. Kinetics were measured by comparing the ketal monomer and ketone by-product peak integrations at various time intervals. **Figure 2**a demonstrates the progression of hydrolysis for monomer 3 in pD 5.0 buffer solution, where a decrease in the ketal methyl peak intensity at 1.31 ppm was observed along with a concomitant increase in the acetone methyl peaks at 2.13 ppm over time. All monomers exhibited first-order degradation kinetics, as illustrated in the pH-dependent degradation profiles shown in Figure 2b,c. The hydrolysis half-lives ($t_{1/2}$) for monomers 3, 5, and 7 at pD 5.5 were 23.2, 45.2, and 167 h, respectively. As expected, the $t_{1/2}$ value for each monomer significantly increased at pD 7.4 (**Table 1**).[15] The observed trends in hydrolysis kinetics are dictated by the relative change in steric strain from the sp^3 ground state to the sp^2 transition state, according to the well-established ketal hydrolysis mechanism.[45] Whereas the dimethyl and cyclopentyl ketals of monomers 3 and 5 release torsional strain[12,15,19,25] from the ground to the transition state (**Figure 3**a), the cyclohexyl ketal of monomer 7 undergoes an increase in torsional strain energy (Figure 3b), thus exhibiting a significantly decrease in hydrolysis rate.[15] The trends in ketal stability reported herein are in good agreement with the fundamental study of ketal protecting groups reported by Kreevoy et al., which established a similar order of stability for ethoxy protected acetone, cyclopentanone, and cyclohexanone,[15] as well as more recent work on similar ketal linkages reported by Shenoi et al.[25] and Liu et al.[19]

2.3. Photopolymerization Kinetics

Figure 4a illustrates the synthesis of degradable poly(β-thioether ester ketal) thermosets using monomers 3, 5, or 7 with pen-

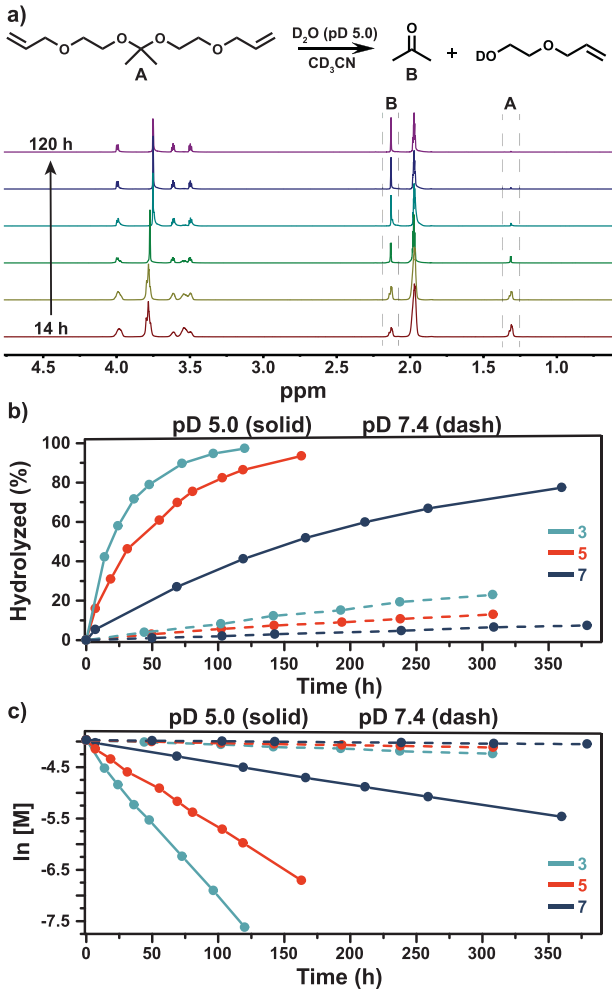

Figure 2. a) 1H-NMR of monomer 3 in pD 5.0 deuterated buffer from 14 h to 120 h. b) First-order hydrolysis kinetics of monomers 3, 5, and 7 in pD 5.0 and pD 7.4 deuterated buffers with c) the corresponding natural log (monomer concentration) versus time plots.

Table 1. Summary of monomer hydrolysis kinetics.

Monomer	K [h^{-1} x 10^{-4}] pD 5.0	$t_{½}$ [h] pD 5.0	K [h^{-1} x 10^{-4}] pD 7.4	$t_{½}$ [h] pD 7.4
3	300 ± 16.4	23.2 ± 1.24	8.55 ± 0.461	813 ± 44.7
5	154 ± 12.1	45.2 ± 3.65	4.70 ± 0.181	1480 ± 56.7
7	41.5 ± 0.289	167 ± 1.16	2.15 ± 0.203	3240 ± 294

taerythritol tetrakis(3-mercaptopropionate) (PETMP) via thiol-ene photopolymerization. Darocur 1173 was employed as the photoinitiator with a λ_{max} = 365 nm light source. Photopolymer resins were formulated under solvent-free conditions using a 1:1 alkene to thiol stoichiometry. Photopolymerization kinetics of each network were tracked via real-time FTIR (RT-FTIR) to ensure complete conversion of each network composition. Resins for 3P–7P were prepared and sandwiched between two salt plates using a minimal amount of resin. After establishing a baseline for FTIR, UV light exposure (15.0 mW cm^{-2}) was initiated, and functional group conversion was determined by measuring the change in thiol (2557 cm^{-1}, Figure 4b) and alkene (1646 cm^{-1}, Figure 4c) peaks over time. Figure 4d shows a representative kinetic profile for the 7/PETMP system for which 95% conversion was obtained after 130 s of UV exposure. The stoichiometric consumption of both alkene and thiol function-

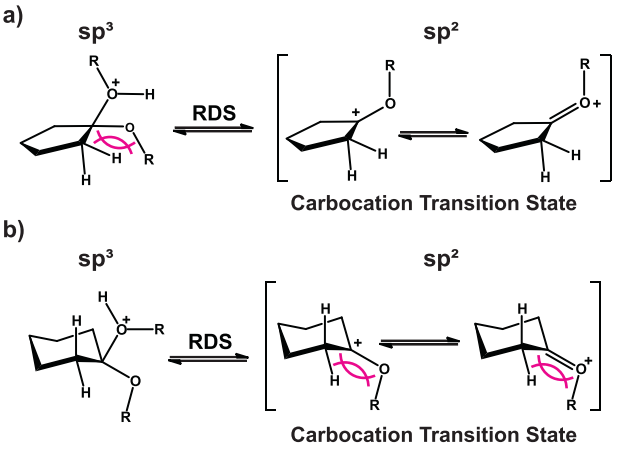

Figure 3. The rate-determining step (RDS) of the acid-catalyzed ketal hydrolysis mechanism is represented by monomers a) 5 and b) 7, where the structure undergoes an sp^3 to sp^2 hybridization change from the ground to the transition state.

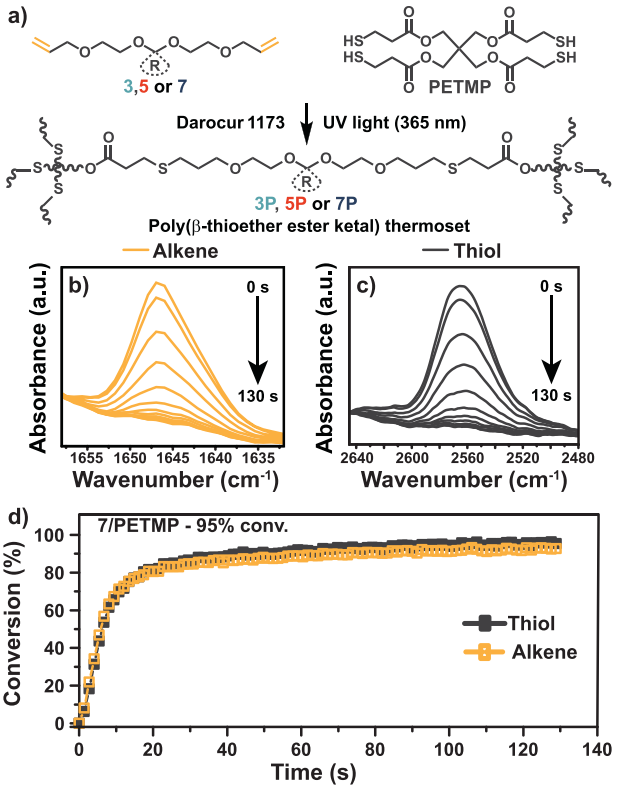

Figure 4. a) Synthesis scheme of poly(β-thioether ester) thermosets from monomers 3, 5, and **7** with PETMP and Darocur 1173 photoinitiator. Change in b) alkene and c) thiol peak areas at 1646 cm^{-1} and 2557 cm^{-1} over time. d) RT-FTIR photopolymerization kinetics of monomer **7** and PETMP based on thiol and alkene conversion versus time from 0 to 130 s.

alities suggests an ideal step-growth polymerization with minimal homopolymerization of alkene groups or competing side reactions between thiol and ketal functionalities. As illustrated in Figure S16 (Supporting Information), similar kinetic profiles and functional group conversions >95% were observed for all other monomers with PETMP.

2.4. Polymer Network Characterization

Differential scanning calorimetry (DSC), dynamic mechanical analysis (DMA), and tensile mechanical testing were utilized to elucidate the influence of ketal monomer structure on thermomechanical and mechanical properties of the polymer networks. Differential scanning calorimetry was initially employed to measure the glass transition temperature (T_g) of each network and to identify any other thermal transitions. T_g was identified by a single second-order endotherm present in each thermogram at -32.9 °C, -29.0 °C, and -19.0 °C for 3P, 5P, and 7P, respectively (**Figure 5**a). While 3P and 5P shared similar T_g values, the significant increase in T_g of 7P is attributed to the increased bulkiness of the cyclohexyl group pendent to the backbone of the polymer network.[46] Figure 5b shows the storage moduli (E') and tan δ (E'/E'') curves for polymer networks 3P–7P. In general, T_g values obtained from the peak of the tan δ peaks followed similar trends as previously observed with DSC. Furthermore, DMA revealed narrowly distributed tan δ curves (FWHM $\leq$ 10.5 °C), indicating well-defined, homogenous networks that are typical of thermosets formed from the thiol-ene step-growth polymerization. Additionally, all samples exhibited near-identical rubbery moduli suggesting similar cross-link densities—a result expected given the similar molecular dimensions among the library of bisallyl monomers. The structure of the ketal monomer did not exert significant changes in the glassy or rubbery moduli, as indicated in Figure 5b. Figure 5c shows the stress–strain curves for each polymer thermoset from which Young's modulus, strain at break, and other values are quantified in **Table 2**. As indicated, tensile testing showed similar Young's moduli for all three thermoset samples (2.39–2.76 MPa) and was within the typical range of other thiol–ene network materials.[47] While the strain at break from 3P appears to be greater than the other samples, it also had the highest standard deviation (Table 2). Statistical analysis using a two-tailed *t*-test ($\alpha = 0.05$) revealed no significant difference in the strain at the break between the three networks. We speculate that the highly flexible thioether linkages dictate the overall formulated under solvent-free conditions using influence from the ketal linkages—an observation that agrees well with our previous work using cyclic ketal building blocks.[30] Thermogravimetric analysis, as provided in Figure 5d, showed similar thermal degradation profiles for 3P–7P, with 10% mass loss temperatures ($T_{d,\,10\%}$) observed at 250, 292, and 285 °C for 3P, 5P, and 7P, respectively (Table 2). The major thermolysis transition occurred from ≈300 to 500 °C with no measured or visible char remaining after complete degradation (Figure 5d).

2.5. Thermoset Degradation

Hydrolytic degradation of polymer thermosets is directly influenced by a complex set of variables including hydrolytic stabil-

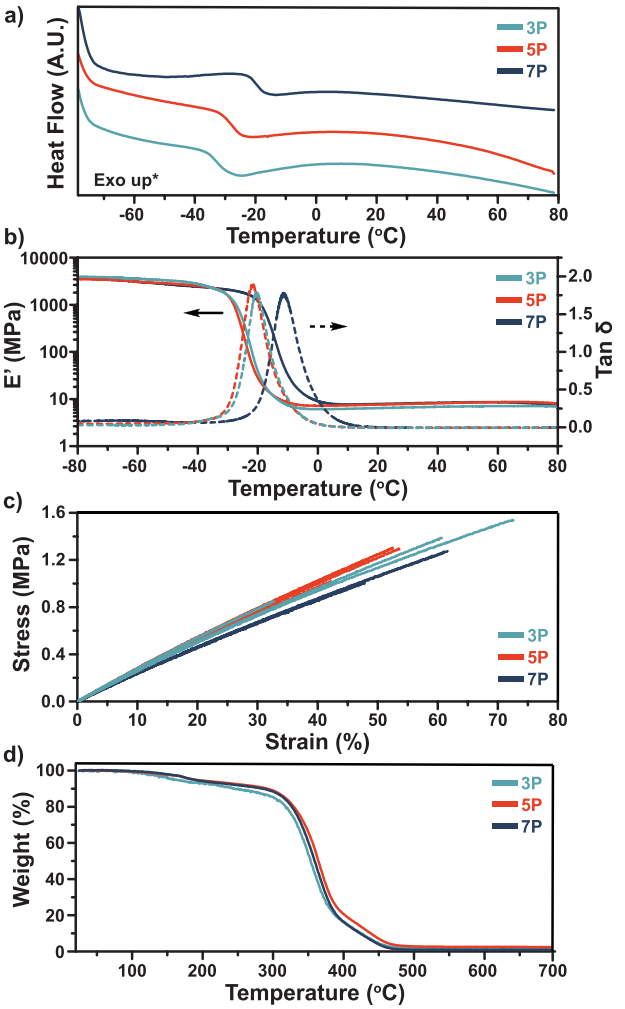

Figure 5. a) Glass transition endotherms of 3P–7P measured via DSC experiments. b) DMA experiments depicting storage modulus and tan δ measurements of 3P–7P. c) Stress versus Strain measurements of 3P–7P via ASTM D638 tensile testing. d) TGA profiles of 3P–7P measured in air atmosphere.

Table 2. Summary of mechanical, thermomechanical, and thermal degradation data.

	Networks		
Properties	**3P**	**5P**	**7P**
Young's Modulus [MPa]	2.69 ± 0.139	2.77 ± 0.0652	2.39 ± 0.00720
Strain at Break (mm/mm)	55.3 ± 20.38	49.4 ± 6.24	56.7 ± 7.89
Peak Stress (MPa)	1.26 ± 0.362	1.20 ± 0.157	1.18 ± 0.155
Peak Load (N)	5.53 ± 1.46	5.23 ± 0.717	5.26 ± 0.788
T_g DSC [°C]	-32.9	-29.0	-19.0
T_g DMA [°C]	-19.5 ± 0.710	-22.1 ± 0.230	-10.8 ± 0.650
Glassy Modulus [MPa, −80 °C]	4027 ± 82.7	3605 ± 206	3640 ± 332
Rubbery Modulus (MPa, 25 °C)	6.54 ± 0.370	7.59 ± 0.190	7.89 ± 0.070
FWHM [tan δ]	9.38 ± 0.39	9.76 ± 0.13	10.51 ± 0.40
$T_{d,\,10\%}$ [°C]	250	292	285

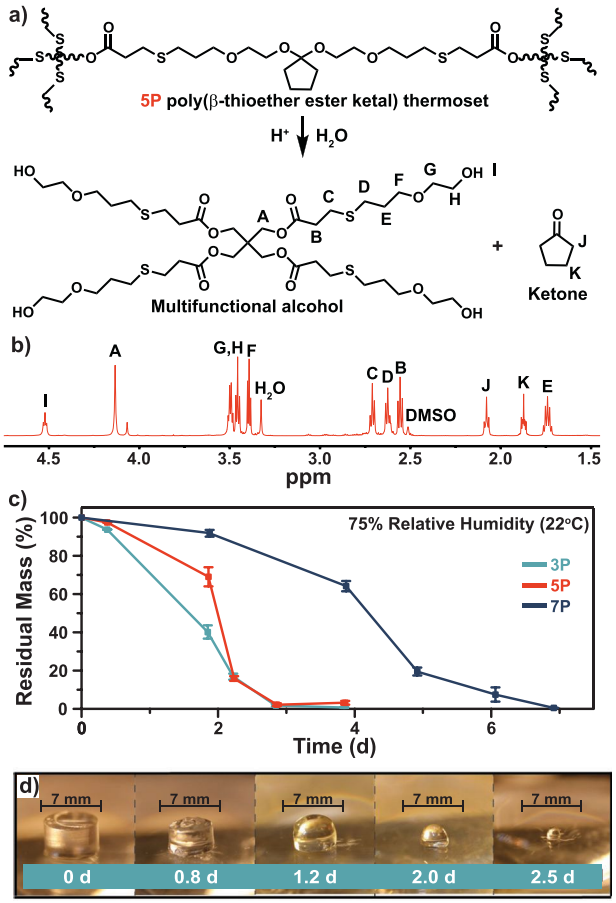

Figure 6. a) Degradation of poly(*β*-thioether ester ketal) thermosets into alcohol and ketone by-products. b) ^{1}H NMR of the mixture of degradation by-products for 5P. c) Mass-loss of 3P–7P samples at 75% relative humidity. d) Surface dominant erosion of a 3P sample at 75% relative humidity. Note: Degradation by-products were wicked from the samples via an absorbant pad prior to the capture of pictures.

ity of the network building blocks, hydrophobicity of the polymer network, diffusion of water into the network, and miscibility and diffusion of degradation by-products into the surrounding medium. **Figure 6**a shows the general scheme for hydrolytic degradation of our poly(*β*-thioether ester ketal) thermosets—a process that results in the formation of multifunctional alcohol and ketone by-products. The structure of the by-products was confirmed by ^{1}H NMR, as exemplified in Figure 6b following degradation of the 5P sample. The composition of these by-products suggests ketal hydrolysis to be the sole mechanism of degradation, ruling out any major contribution from ester hydrolysis on the experimental timescale. With PETMP serving as a common multifunctional building block for all three networks, any variation in hydrophobicity of the thermosets would be attributed to the ketal building blocks. As may be expected, all three thermosets showed similar hydrophobic characteristics as indicated by similar static water contact angle values (Figure S17, Supporting Information, 3P: 83.3°, 5P: 81.9°, and 7P: 81.7°); thus, hydrophobicity likely plays a minimal role in the observed differences in mass-loss profiles. The miscibility of the degradation by-products with water varies depending on the chemical structure (e.g., acetone is miscible whereas cyclopentanone and cyclohexanone are mostly immiscible). The tetrafunctional alcohol also displays low miscibility with water. Despite these variations in miscibility leading to solution heterogeneities during degradation, we decided to perform degradation experiments in a fully aqueous environment to avoid complications associated with network swelling when employing organic cosolvents in the degradation media. When conducting our initial exploratory experiments, we observed that preparation of the photopolymer resins and polymerization under ambient laboratory conditions resulted in high batch-to-batch variability with regards to degradation times. While the batch-to-batch variability is likely a consequence of differences in relative humidity within the lab during sample preparation, these observations prompted an initial investigation of poly(*β*-thioether ester ketal) thermoset degradation under constant humidity. To qualitatively measure the effect of humidity on network degradation, a controlled mass-loss degradation experiment was implemented by placing 3.75 mm × 6.50 mm thermoset disks in a saturated sodium chloride humidity chamber (75% relative humidity) at 22 °C. Samples were removed at specific time intervals from the chamber, degradation by-products were wicked away, and then the disks were weighed to determine relative mass loss. As shown in Figure 6c, the overall trends in network degradation adhere to trends observed for hydrolytic stability of the ketal linkages (e.g., time to full mass loss increases in the order of 3P, 5P, and 7P). A surface dominant erosion behavior was also observed for all three thermoset compositions, as exemplified by photographs of 3P versus time in Figure 6c.

To mitigate variations due to humidity, samples for evaluation under acidic and neutral aqueous conditions were prepared and stored in a nitrogen-purged glovebox prior to use. As shown in **Figure 7**a, the degradation profiles in acetate buffer (pH 4.07, 30 °C) exhibit a strong dependence on the structure of the ketal linker. Immediate onset of mass loss was observed for the acetone-based ketal 3P network with complete degradation within 1.5 days. In contrast, the 7P network derived from the cyclohexanone-based ketal required >10 days to reach full degradation. Similar degradation trends were observed in PBS buffer (pH 7.40, 30 °C, Figure 7b). To investigate the polymer erosion process under immersion conditions, an accelerated degradation experiment was conducted with optical microscopy using 3.5 mm × 0.75 mm sample disks and a 0.01 M HCl solution. Albeit on a much shorter timescale due to the lower pH and the decrease in sample thickness, the samples degraded according to the same trends observed in the previous buffer solutions, e.g., 3P degraded at the fastest rate followed by 5P and 7P (Figure 7c). A decrease in sample dimensions while generally maintaining sample shape is indicative of a surface-dominant polymer erosion process. Surface erosion is a consequence of hydrolysis kinetics being faster than water ingress into the bulk of the material.[48–50] The surface erosion behavior of 3P–7P is consistent with previous ketal-based thermosets.[30,51]

3. Conclusion

Radical-mediated thiol-ene photopolymerization was implemented to fabricate hydrolytically degradable poly(*β*-thioether ester ketal) networks derived from three diallyl acyclic ketal

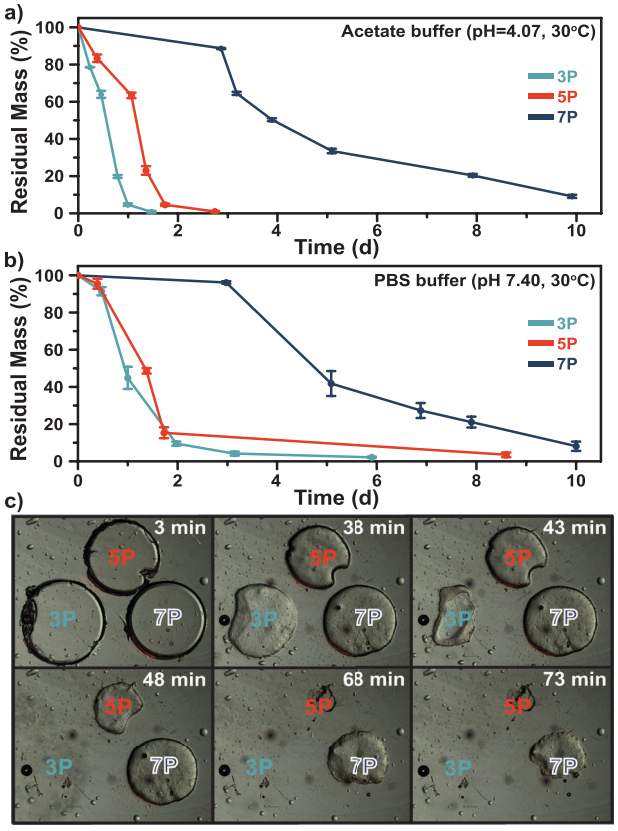

Figure 7. Mass-loss of 3P–7P samples in a) acidic acetate buffer (pH 4.07) and b) neutral PBS buffer (pH 7.40). c) Optical microscopy of 3.5 mm × 0.75 mm (diameter × thickness) sample disks in 70% 0.01 M HCl at various time intervals.

monomers and a commercially available multifunctional thiol. Using optical microscopy and mass-loss experiments, samples were shown to under a surface dominant erosion in the presence of water vapor (75% relative humidity), as well as in acidic and neutral solutions. Hydrolytic stability, under all investigated conditions, was shown to be dependent on ketal structure, exhibiting an order of increasing stability of dimethyl ketal (**3P**), cyclopentyl ketal (**5P**), and cyclohexyl ketal (**7P**). Analysis of degradation by-products via ^{1}H-NMR confirmed ketal hydrolysis to be the primary mode of hydrolytic degradation with no detectable ester hydrolysis. The tunable degradation behavior of the poly(*β*-thioether ester ketal) networks gives them great potential in various applications that require complete and controlled degradation such as therapeutic drug release, sacrificial coatings, or adhesives.

4. Experimental Section

Materials: All reagents were obtained commercially and used without further purification unless otherwise specified. Cyclopentanone and 2-allyloxyethanol were sourced from TCI Chemical. Cyclohexanone and 4 Å molecular sieves were sourced from Acros Organics; 2-hydroxy-2-methylpropiophenone (Darocur 1173) was sourced from Ciba; pentaerythritol tetrakis(3-mercaptopropionate) (PETMP) was sourced from Bruno Bock; p-toluenesulfonic acid (p-TsOH) and phosphate-buffered saline were sourced from Sigma–Aldrich. All other solvents and chemicals were obtained from Fisher Scientific. Acetate buffer (pH 4.07) was made by mixing 2 L of 0.1 M acetic acid with 439.0 ml of 0.1 M sodium acetate. pD 7.4 0.1 M PBS/D_2O buffer was made by adding 154 mg of $Na_2HPO_4{\cdot}7H_2O$ + 58 mg $NaH_2PO_4H_2O$ to 10 mL of D_2O.

Monomer characterization: Monomer structure and purity was confirmed using ^{1}H-NMR, ^{13}C-NMR, COSY, and HSQC NMR experiments using a Bruker Avance™ 600 MHz spectrometer. NMR samples were prepared in either deuterated chloroform or deuterated dimethyl sulfoxide. Additionally, monomer structure was confirmed by mass spectrometry using a Bruker 12 Tesla APEX–Qe FTICR-MS in positive-ion mode ionization with an Apollo II ion source.

Synthesis of Monomer 3: Eleven grams of (0.189 mol) acetone, 72.0 g (0.705 mol) 2-allyloxyethanol, 50.0 ml THF, and 30.0 g of 4 Å molecular sieves were added to a 500 mL round bottom flask with a stir bar and purged with nitrogen for 30 min. After purging, 0.2 mL of concentrated sulfuric acid was injected to the reaction via syringe and left to stir for 15 h at room temperature. The reaction was subsequently quenched with 5.0 mL triethylamine, filtered to remove the molecular sieves and rotary evaporated to remove any THF. Two hundred milliliters of diethyl ether was then added to the remaining product, washed twice with sodium bicarbonate and dried over anhydrous sodium sulfate. All solvent was then removed from the reaction by vacuum to yield the crude product. The pure product was isolated by flash chromatography using an eluent system of ethyl acetate and hexanes (10:90) +5% triethylamine. The collected fractions were rotary evaporated and left under a high vacuum for 10 h to yield 7.34 g of clear oil. (Yield:15.9%) ^{1}H NMR (600 MHz, DMSO-d6) δ 5.88 (ddt, J = 17.3, 10.5, 5.2 Hz, 2H), 5.27 (q, J = 1.8 Hz, 1H), 5.24 (q, J = 1.8 Hz, 1H), 5.14 (q, J = 1.6 Hz, 1H), 5.12 (q, J = 1.6 Hz, 1H), 3.96 (dt, J = 5.3, 1.6 Hz, 4H), 3.53 – 3.48 (m, 8H), 1.29 (s, 6H).^{13}C NMR (151 MHz, DMSO-d6) δ 135.72 (CH), 116.35 (CH_2), 99.73 (C), 71.49 (CH_2), 69.60 (CH_2), 60.08 (CH_2), 25.08 (CH_3). *m/z*: 267.156680, measured: 267.156755.

Synthesis of Monomer 5: Seventeen grams of (0.202 mol) cyclopentanone, 42.0 g (0.411 mol) 2-allyloxyethanol, 40.0 mL THF, and 55.0 g of 4 Å molecular sieves were added to a 500 ml round bottom flask with a stir bar and purged with nitrogen for 30 min. After purging, 0.2 mL of concentrated sulfuric acid was injected into the reaction via syringe and left to stir for 15 h at room temperature. The reaction was subsequently quenched with 5.0 mL triethylamine, filtered to remove the molecular sieves and rotary evaporated to remove the THF. Two hundred milliliters of diethyl ether was then added to the remaining product, washed twice with sodium bicarbonate, and dried over anhydrous sodium sulfate. All solvent was then removed from the reaction by vacuum to yield the crude product. The pure product was isolated by flash chromatography using an eluent system of ethyl acetate and hexanes (10:90) +5% triethylamine. The collected fractions were rotary evaporated and left under a high vacuum for 10 h to yield 5.97 g of clear oil. (Yield:10.9%) ^{1}H NMR (600 MHz, Chloroform-d) δ 5.95–5.86 (m, 2H), 5.28 (q, J = 1.7 Hz, 1H), 5.25 (q, J = 1.7 Hz, 1H), 5.17 (q, J = 1.6 Hz, 1H), 5.15 (q, J = 1.6 Hz, 1H), 4.05–4.00 (m, 4H), 3.64–3.60 (m, 4H), 3.60–3.56 (m, 4H), 1.85–1.78 (m, 4H), 1.70–1.61 (m, 4H).^{13}C NMR (151 MHz, Chloroform-d) δ 134.96 (CH), 116.68 (CH_2), 112.08 (C), 72.13 (CH_2), 69.65 (CH_2), 61.32 (CH_2), 34.77 (CH_2), 23.04 (CH_2). *m/z*: 293.172330, measured: 293.172473.

Synthesis of Monomer 7: Two grams of (0.204 mol) cyclohexanone, 42.0 g (0.411 mol) 2-allyloxyethanol, 58.0 ml THF, and 55.0 g of 4 Å molecular sieves were added to a 500 mL round bottom flask with a stir bar and purged with nitrogen for 30 min. After purging, 0.2 mL of concentrated sulfuric acid was injected into the reaction via syringe and left to stir for 15 h at room temperature. The reaction was subsequently quenched with 5.0 mL triethylamine, filtered to remove the molecular sieves and rotary evaporated to remove the THF. Two hundred milliliters of diethyl ether was then added to the remaining product, washed twice with sodium bicarbonate, and dried over anhydrous sodium sulfate. All solvent was then removed from the reaction by vacuum to yield the crude product. The pure product was isolated by flash chromatography using an eluent system of ethyl acetate and hexanes (10:90) +5% triethylamine. The collected fractions were rotary evaporated and left under a high vacuum for 10 h to yield 13.1 g of a clear oil. (Yield:22.7%) ^{1}H NMR (600 MHz, Chloroform-d) δ 5.96–5.85 (m, 2H), 5.29 (p, J = 1.6 Hz, 1H), 5.26 (p, J = 1.7 Hz, 1H), 5.18–5.16

(m, 1H), 5.16–5.13 (m, 1H), 4.05–4.01 (m, 4H), 3.62–3.55 (m, 4H), 1.67 (t, $J = 5.8$ Hz, 4H), 1.51 (p, $J = 5.9$ Hz, 4H), 1.39 (q, $J = 5.9$ Hz, 2H). ^{13}C NMR (151 MHz, Chloroform-d) δ 135.01 (CH), 116.60 (CH_2), 100.23 (C), 72.11 (CH_2), 69.72 (CH_2), 59.22 (CH_2), 33.63 (CH_2), 25.61 (CH_2), 22.94 (CH_2). *m/z*: 307.187980, measured: 307.187883.

Monomer Hydrolysis Kinetics: For monomers 3, 5, and 7, 0.75 mL of 25×10^{-3} M CD_3CN monomer solution was mixed with 0.25 mL of acetate/D_2O buffer (pD 5.0) or PBS/D_2O buffer (pD 7.4) for a final monomer concentration of 0.0185 M. Overall monomer hydrolysis was measured via ^{1}H-NMR by comparing ketal and ketone signal intensities at various time intervals. First-order rate constants (K) and half-life values ($t_{1/2}$) were measured from the natural logarithm of ketal concentration versus time plots for each monomer and buffer solution.

Polymer Network Synthesis: PETMP and monomer were mixed at a 1:1 ratio (thiol:alkene) with 3 mol% Darocur 1173 photoinitiator. The solution was mixed using a vibratory mixer, centrifuged, degassed under high vacuum for 5 s, and sealed before being transferred to a nitrogen-purged glovebox. Inside the glovebox, the uncured resin was transferred to a PDMS mold and exposed to a medium pressure UV lamp (10 mW cm^{-2}) for 3 min. Thermoset samples were then stored in the glovebox until later use to prevent onset hydrolysis.

Photopolymerization Kinetics: Polymerization kinetics were measured by real-time FTIR spectroscopy using a Nicolet 8700 FTIR spectrometer with a KBr beam splitter and MCT/A detector. Experiments consisted of sandwiching ≈20 µL of uncured resin between two salt plates before being in the beam path of the instrument. Data acquisition (2 scans s^{-1}/4 cm^{-1} resolution) was started simultaneously to UV exposure (15.0 mW cm^{-2}) using an Omnicure Series 1000 light source. The conversion was monitored by integrating the thiol (2557 cm^{-1}) and allyl (1646 cm^{-1}) peak areas over ≈130 s.

Humidity Degradation Experiments: Degradation sample disks of ≈3.75 mm × 6.50 mm (160 mg) were placed in a humidity chamber regulated by a saturated sodium chloride bath (75% relative humidity) at 22 °C. Samples were placed on individual pads constructed of a Kim Wipe tissue topped with cheesecloth to wick away degradation by-products. At specific time intervals, samples were removed in triplicate from the humidity chamber, washed with water and acetone, placed under high vacuum for at least 4 h to dry, and weighed via microbalance. The average mass for each time interval was then to construct a residual mass versus time plot for each thermoset composition and degradation solution.

Mass-Loss Degradation Experiments: Degradation sample disks of ≈3.75 mm × 6.50 mm (160 mg) were placed in individual 20 mL vials, filled with degradation solution, and placed in an incubation chamber at 30 °C. At specific time intervals, samples would be removed in triplicate, decanted of their solution, and washed with acetone and water 2× each to remove insoluble degradation by-products. The samples were then frozen in their respective vials using liquid nitrogen and lyophilized to remove all water from the sample. After 48 h, the dry mass of each sample was measured via microbalance and then used to construct residual mass versus time plots. This process was repeated for each thermoset composition and degradation solution.

Optical Microscopy: Optical microscopy of degradation experiments was performed on a Nikon SMZ800N microscope using a Moticam 1080 camera and software. Degradation videos were constructed through the compilation of multiple microscopy images.

Differential Scanning Calorimetry: DSC experiments were performed on a TA Instruments Q100 for each thermoset composition using TA instruments Tzero™ aluminum pans. Experiments consisted of heat/cool/heat cycles from −80.0 to 80.0 °C using a 10.0 °C min^{-1} heating rate and 5.0 °C min^{-1} cooling rate.

Dynamic Mechanical Analysis: DMA experiments were performed on a TA Instruments Q800 using samples of approximate dimensions of 20.0 mm × 5.00 mm × 1.00 mm (length × width × thickness). Experiments consisted of a temperature ramp from −80.0 to 80.0 °C using a constant frequency of 1.0 Hz, a strain rate of 0.05%, and a 2.0 °C min^{-1} ramp rate in tension mode. All experiments were performed in triplicate to ensure consistent sample measurements.

Thermogravimetric Analysis: TGA experiments were performed on a TA Instruments Q500™ using a platinum pan and thin-film thermoset samples of ≈8.0 mg each. Experiments consisted of a temperature ramp of 10 °C min^{-1} up to a final temperature of 600 °C in air atmosphere conditions.

Mechanical Testing: Tensile testing was conducted in accordance with ASTM D638 utilizing a Type V tensile bar with a gauge length of 7.62 mm, a gauge width of 3.18 mm, and an overall thickness of 1.41 mm. Samples were tested on an MTS Insight electromechanical test frame with a 500 N load cell at a constant crosshead speed of 1.52 mm min^{-1} to failure. Testing of each thermoset type was performed in at least triplicate to ensure consistent and accurate measurements.

Supporting Information

Supporting Information is available from the Wiley Online Library or from the author.

Acknowledgements

The authors acknowledge financial support from the National Science Foundation (CHE-1710589). BMA acknowledges traineeship support from the NSF Research Traineeship "Interface" program (DGE-1449999) through the University of Southern Mississippi. K.D.K. acknowledges support from the NSF REU Site: Polymer Innovation for a Sustainable Future (DMR-1659340).

Conflict of Interest

The authors declare no conflict of interest.

Data Availability Statement

The data that support the findings of this study are available from the corresponding author upon reasonable request.

Keywords

degradable, hydrolysis, ketal, thermosets, thiol-ene photopolymerization

Received: January 13, 2022
Revised: February 2, 2022
Published online:

[1] B. Dellago, A. Ricke, T. Geyer, R. Liska, S. Baudis, *Eur. Polym. J.* **2021**, *154*, 110536.
[2] U. Edlund, A. C. Albertsson, *Degradable Aliphatic Polyesters*, Springer Berlin Heidelberg, Berlin, Heidelberg **2002**, pp. 67–112.
[3] S. Binauld, M. H. Stenzel, *ChemComm.* **2013**, *49*, 2082.
[4] G. Seetharaman, A. R. Kallar, V. M. Vijayan, J. Muthu, S. Selvam, *J. Colloid Interface Sci.* **2017**, *492*, 61.
[5] C. R. Nuttelman, S. M. Henry, K. S. Anseth, *Biomaterials* **2002**, *23*, 3617.
[6] M. Fujimoto, M. Isobe, S. Yamaguchi, T. Amagasa, A. Watanabe, T. Ooya, N. Yui, *J. Biomater. Sci., Polym. Ed.* **2005**, *16*, 1611.
[7] K. S. Anseth, D. C. Svaldi, C. T. Laurencin, R. Langer, in *Photopolymerization*, American Chemical Society, **1997**, *673*, pp. 189–202.

[8] K. S. Anseth, V. R. Shastri, R. Langer, *Nat. Biotechnol.* **1999**, *17*, 156.
[9] K. L. Poetz, H. S. Mohammed, D. A. Shipp, *Biomacromolecules* **2015**, *16*, 1650.
[10] K. L. Poetz, H. S. Mohammed, B. L. Snyder, G. Liddil, D. S. K. Samways, D. A. Shipp, *Biomacromolecules* **2014**, *15*, 2573.
[11] S. Ma, D. C. Webster, *Prog. Polym. Sci.* **2018**, *76*, 65.
[12] E. H. Cordes, H. G. Bull, *Chem. Rev.* **1974**, *74*, 581.
[13] K. E. Uhrich, A. Gupta, T. T. Thomas, C. T. Laurencin, R. Langer, *Macromolecules* **1995**, *28*, 2184.
[14] D. A. Shipp, C. W. McQuinn, B. G. Rutherglen, R. A. McBath, *ChemComm.* **2009**, 6415.
[15] M. M. Kreevoy, C. R. Morgan, R. W. Taft, *J. Am. Chem. Soc.* **1960**, *82*, 3064.
[16] V. Bulmus, Y. Chan, Q. Nguyen, H. L. Tran, *Macromol. Biosci.* **2007**, *7*, 446.
[17] S. Chatterjee, S. Ramakrishnan, *Macromolecules* **2011**, *44*, 4658.
[18] D. Huang, F. Yang, X. Wang, H. Shen, Y. You, D. Wu, *RSC Polym. Chem* **2016**, *7*, 6154.
[19] B. Liu, S. Thayumanavan, *J. Am. Chem. Soc.* **2017**, *139*, 2306.
[20] D. N. Amato, D. V. Amato, O. V. Mavrodi, W. B. Martin, S. N. Swilley, K. H. Parsons, D. V. Mavrodi, D. L. Patton, *ACS Macro Lett.* **2017**, *6*, 171.
[21] D. V. Amato, D. N. Amato, L. T. Blancett, O. V. Mavrodi, W. B. Martin, S. N. Swilley, M. J. Sandoz, G. Shearer, D. V. Mavrodi, D. L. Patton, *Acta Biomater.* **2018**, *67*, 196.
[22] M. J. Heffernan, N. Murthy, *Bioconjug. Chem.* **2005**, *16*, 1340.
[23] S. Lee, S. C. Yang, M. J. Heffernan, W. R. Taylor, N. Murthy, *Bioconjug. Chem.* **2007**, *18*, 4.
[24] V. F. Fiore, M. C. Lofton, S. Roser-Page, S. C. Yang, J. Roman, N. Murthy, T. H. Barker, *Biomaterials* **2010**, *31*, 810.
[25] R. A. Shenoi, J. K. Narayanannair, J. L. Hamilton, B. F. L. Lai, S. Horte, R. K. Kainthan, J. P. Varghese, K. G. Rajeev, M. Manoharan, J. N. Kizhakkedathu, *J. Am. Chem. Soc.* **2012**, *134*, 14945.
[26] R. A. Shenoi, B. F. L. Lai, M. Imran ul-haq, D. E. Brooks, J. N. Kizhakkedathu, *Biomaterials* **2013**, *34*, 6068.
[27] S. Maity, P. Choudhary, M. Manjunath, A. Kulkarni, N. Murthy, *ChemComm.* **2015**, *51*, 15956.
[28] G. - H. Choi, D. Y. Hwang, D. H. Suh, *Macromolecules* **2015**, *48*, 6839.
[29] S. Lingier, Y. Spiesschaert, B. Dhanis, S. De Wildeman, F. E. Du Prez, *Macromolecules* **2017**, *50*, 5346.
[30] B. M. Alameda, T. C. Palmer, J. D. Sisemore, N. G. Pierini, D. L. Patton, *RSC Polym. Chem.* **2019**, *10*, 5635.
[31] S. Kim, O. Linker, K. Garth, K. R. Carter, *Polym. Degrad. Stab.* **2015**, *121*, 303.
[32] H. T. T. Duong, C. P. Marquis, M. Whittaker, T. P. Davis, C. Boyer, *Macromolecules* **2011**, *44*, 8008.
[33] E. J. Kepola, C. S. Patrickios, *Macromol. Chem. Phys.* **2018**, *219*, 1700404.
[34] J. A. Syrett, D. M. Haddleton, M. R. Whittaker, T. P. Davis, C. Boyer, *ChemComm.* **2011**, *47*, 1449.
[35] S. E. Paramonov, E. M. Bachelder, T. T. Beaudette, S. M. Standley, C. C. Lee, J. Dashe, J. M. J. Fréchet, *Bioconjug. Chem.* **2008**, *19*, 911.
[36] S. D. Khaja, S. Lee, N. Murthy, *Biomacromolecules* **2007**, *8*, 1391.
[37] S. Guo, Y. Nakagawa, A. Barhoumi, W. Wang, C. Zhan, R. Tong, C. Santamaria, D. S. Kohane, *J. Am. Chem. Soc.* **2016**, *138*, 6127.
[38] B. T. Whiting, G. W. Coates, *J. Am. Chem. Soc.* **2013**, *135*, 10974.
[39] E. Schopf, J. Sankaranarayanan, M. Chan, R. Mattrey, A. Almutairi, *Mol. Pharm.* **2012**, *9*, 1911.
[40] S. L. Buchwalter, L. L. Kosbar, *J. Polym. Sci. A Polym. Chem.* **1996**, *34*, 249.
[41] S. Bhaladhare, S. Kim, K. R. Carter, *ACS Appl. Polym. Mater.* **2019**, *1*, 2846.
[42] M. Burek, S. Waśkiewicz, A. Lalik, I. Wandzik, *RSC Polym. Chem* **2018**, *9*, 3721.
[43] H. Pohlit, D. Leibig, H. Frey, *Macromol. Biosci.* **2017**, *17*, 1600532.
[44] M. Burek, M. Kowalczyk, Z. P. Czuba, W. Krol, R. Pilawka, S. Waskiewicz, *Polym. Degrad. Stab.* **2016**, *129*, 296.
[45] N. Leber, L. Kaps, M. Aslam, J. Schupp, A. Brose, D. Schäffel, K. Fischer, M. Diken, D. Strand, K. Koynov, A. Tuettenberg, L. Nuhn, R. Zentel, D. Schuppan, *J. Control. Release* **2017**, *248*, 10.
[46] J. Karger-Kocsis, O. Gryshchuk, N. Jost, *J. Appl. Polym. Sci.* **2003**, *88*, 2124.
[47] B. T. Good, S. Reddy, R. H. Davis, C. N. Bowman, *Sens. Actuators, B* **2007**, *120*, 473.
[48] J. A. Tamada, R. Langer, *Proc. Natl. Acad. Sci. U.S.A.* **1993**, *90*, 552.
[49] A. Göpferich, *Biomaterials* **1996**, *17*, 103.
[50] F. v. Burkersroda, L. Schedl, A. Göpferich, *Biomaterials* **2002**, *23*, 4221.
[51] G. Herwig, A. P. Dove, *ACS Macro Lett.* **2019**, *8*, 1268.

